Broadband airfoil trailing-edge noise prediction from measured surface pressures and spanwise length scales

Andreas Herrig, M. Kamruzzaman, W. Würz and S. Wagner

Universität Stuttgart Institute of Aerodynamics and Gas Dynamics (IAG) Pfaffenwaldring 21, 70550 Stuttgart, Germany

In this paper an effective approach to estimate airfoil Turbulent Boundary-Layer Trailing-Edge (TBL-TE) far-field noise from measured surface pressure fluctuations (SPF) is evaluated. Measurements of both SPF and TE noise were performed on a NACA 0012 airfoil of 0.4 m chord at Reynolds numbers of 1.0–1.9 millions for various angles of attack. A non-homogeneously spaced array of five Kulite-sensors near the TE at $x/c = 0.989$ is employed to measure point spectra and spanwise two-point correlations of surface pressure fluctuations. Finally spanwise SPF length-scales are derived as function of frequency. Comparisons to measured TE noise and semi-empirical predictions of surface pressures and far-field noise show very good agreement. It is found, that the proposed method can cover a larger frequency range than standard acoustic measurement techniques. Therefore it can provide valuable assistance in extending spectra obtained conventionally, mainly to low frequencies. Furthermore, pressure and suction side contributions to far-field noise can be obtained separately.

NOMENCLATURE

ROMAN SYMBOLS

b, c = airfoil section span and chord length
c_p = static surface pressure coefficient
d, d^+ = transducer diameter, made dimensionless with wall unit
$G_{p,ff}$ = single-sided sound pressure spectrum in the far-field
G_{pp} = single-sided point power spectral density of wall pressure
$L_{p,ff}$ = far-field sound pressure level re 20 mPa
Ma = free-stream Mach number
$R_{p,ij}$ = two-point correlation index of surface pressure fluctuations
U_e = BL edge velocity
$U_{\bullet}$ = free-stream velocity
x, y, z = streamwise, transverse (wall normal), spanwise coordinate

GREEK SYMBOLS

χ = ratio of scattered sound pressure at TE to hydrodynamic pressure at sensor position
δ_1 = boundary layer displacement thickness
γ_p = coherence of SPFs
$\gamma_{p,ij}$ = coherence of two-point pressure correlations
$\Lambda_{p,3}$ = spanwise length scale of SPFs
τ_w = wall shear stress
φ = polar angle of sound emission from chordwise axis

ACRONYMS

BGN = Background Noise
CPV = Coherent Particle Velocity
IAG = Institute of Aerodynamics and Gas Dynamics
PS = Pressure side
SPF = Surface Pressure Fluctuations
SSPP = Scattered Surface Pressure Prediction
SS = Suction side
TEN = Trailing Edge Noise

1. INTRODUCTION

Quantitative measurement of Turbulent Boundary-Layer Trailing-Edge (TBL-TE) noise in a non-aeroacoustic wind tunnel is a delicate task, as the airfoil

E-mail: {herrig, kamruzzaman, wuerz, wagner}@iag.uni-stuttgart.de

self noise has to be separated from the typically higher background noise (BGN). At the Institute of Aerodynamics and Gas Dynamics (IAG) the Coherent Particle Velocity (CPV) method had been developed [1, 2, 3, 4] for two-dimensional airfoil trailing-edge (TE) noise measurements in such wind tunnels with good aerodynamic quality, i.e. closed test section. It is therefore specifically suited for aeroacoustic validation of low-noise airfoils under well defined aerodynamic boundary conditions.

One of the development objectives of the CPV-method had been the extension of the measurement frequency range at the lower end compared to phased microphone arrays. The difficulty to obtain values in the low-frequency region is the background noise rising strongly at low frequencies, typical for aerodynamic wind tunnels. It masks the low TE noise amplitudes at a short distance from the airfoil. For example in the LWT using the CPV-method it is just possible to resolve the spectral maximum for the NACA 0012 at chord lengths of about 0.4 m, when it is located at about 1 kHz at a free-stream velocity of 60 m/s. But the energy in lower frequency bands can hardly be obtained reliably. Furthermore, the desire to achieve large test Reynolds numbers leads to large airfoil chord lengths, which additionally shift the TE noise spectra to lower frequencies.

Phased microphone arrays as an alternative measurement approach suffer from reduced spatial resolution at low frequencies. To overcome this problem, large aperture and number of microphones are necessary, increasing the costs and efforts of such measurements. Striving for improved spatial resolution of sound sources, the development of cumbersome and time consuming deconvolution algorithms has been progressed recently [5, 6].

However, our interest is on relatively simple test cases, where this spatial resolution to find the source is not needed, e.g. 2d flow with known source position in performance verification of single-element airfoils. Then the suppression of BGN is mainly relevant for measurement accuracy. Beamforming algorithms can recover signals a few decibels below the BGN, limited by the presence of side-lobes in the scan area. So no huge gains in measurement bandwidth at the low frequencies can be expected for the case that TEN and BGN have opposite slopes at the crossover frequency.

Therefore the target of the investigations described in the following is to improve acoustic airfoil verification by obtaining more third-octave bands at or below the frequency of the maximum TE noise level. Because available measurement methods operating with the radiated acoustic field are inherently hampered by the background noise, direct measurements of hydrodynamic quantitities at the noise source (the TE) were considered as a resort. As the hydrodynamic amplitudes are orders of magnitudes larger than the acoustic ones (e.g. fluctuation velocities), much larger BGN to TEN ratios are allowable, before amplitude biasing becomes significant.[1] Having knowledge of the hydrodynamic source properties, a sufficiently accurate theory is necessary to predict TE noise radiated to the far-field. So, indirect measurements of the quantity of interest are performed.

In this study the surface pressure fluctuations (SPF) are considered as the main magnitude causally responsible for TE noise radiation. Knowing the surface pressure spectra, conclusions about the TEN can be drawn, when the "radiation efficiency" and directional characteristic are known.

The idea is intriguingly simple, so of course some previous studies on that topic already exist. Brooks & Hodgson [7] formulated theoretical relations to obtain sound source characteristics

[1]Provided that the flow is not influenced by the high BGN, of course. . .

from the measurement of surface pressure fluctuations and performed validation measurements on a NACA 0012 section of c = 0.61 m chord and b = 0.46 m span with different edge extensions at various Mach numbers Ma = 0.09 – 0.2 in an open-jet aeroacoustic facility. The airfoil was equipped with a large number of 36 pressure transducers, arranged in chordwise and spanwise arrays on both sides of the airfoil as close as x/c = 0.958 to the TE, to determine space-time correlations of the surface pressures. Later, Blake [8] summarized theoretical relations for transferring SPF point spectrum measurements on rigid airfoils to the radiated sound field.

A crucial quantitity is the frequency dependent spanwise length scale of the SPFs, defining the efficiency of scattering at the TE. A simple approach is used in the present paper to measure the length scales with a minimum number of pressure sensors utilizing a non-homogeneously spaced spanwise array.

The possibility and accuracy of far-field noise estimations using these SPF data are examined in this paper by comparison to acoustic measurements and numerical predictions. In section 2 the airfoil section with the pressure transducers used in these tests is described, also explaining aspects of the pressure signal acquisition. Also the prevailing flow-field and test cases are characterized. In the following, in section 3 the SPF point spectrum measurements are described. Comparisons to numerical predictions of point spectra obtained as integral of the wavenumber-frequency spectrum model implemented in the IAGNoise code are performed. After describing the procedure to obtain estimates of the spanwise length scales of pressure fluctuations, the extraction of far-field noise estimates in the current implementation is explained in section 4. Comparisons to acoustic measurements in the same wind tunnel and in an aeroacoustic wind tunnel are performed. Finally aspects of surface vibrations and the influencing of SPFs upstream of the TE by the radiated sound are discussed, as in the acoustic source region a coupling of flow and sound field is present, which raises the question of separation of the two components.

2. EXPERIMENTAL SETUP

2.1. WIND TUNNEL AND AIRFOIL SECTION

The measurements were performed in the Laminar Wind Tunnel (LWT) [9] of the Institute of Aerodynamics and Gas Dynamics (IAG), University of Stuttgart. The LWT is an open return tunnel with a test section of 0.73 m × 2.73 m and 3.15 m length and a turbulence level of $Tu_x \approx 0.02\%$ (f = 20–5000 Hz) at U_∞ = 30 m/s. In the period from May to June 2009 the LWT was modified significantly and equipped with a sound absorbing lining in the diffusor between fan and test section (Fig. 1). The previous inner diffusor wall was removed and the gap filled with coated Basotect acoustic foam of up to 300 mm thickness. Additionally a 3 m long hub silencer was placed infront of the fan. Preliminary hot-wire acoustic measurements showed reductions of narrow-band BGN spectra of about 10–12 dB in a frequency range of 100–4000 Hz. Later in-flow microphone measurements showed reductions of the total sound pressure levels from 94 dBA at 60 m/s to approximately 85 dBA [10]. This is still more than in special acoustic facilities, like e.g. the AWB [11], but enables improved aeroacoustic investigations.

The NACA 0012 airfoil section with a chord length of c = 400 mm and spanwise length of b = 733 mm (designated ‘NA0012_04b’ to distinguish it from other available NACA 0012 models with different chord lengths and trailing-edge

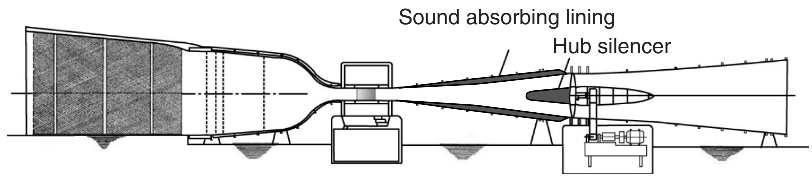

Figure 1: Sketch of LWT equipped with sound absorbing lining in diffusor and hub silencer upstream of fan.

thicknesses) was manufactured at the IAG workshop in CNC machined negative moulds to ensure maximum contour accuracy. Compared to the design coordinates the airfoil sides were rotated minimally around the LE to achieve a sharp trailing-edge of 0.22 ± 0.01 mm thickness (checked with a micrometer screw at several spanwise positions), in order to avoid blunt TE noise. The shells were made of 6 mm thick carbon/glass/carbon laminate. UD carbon layers of 120 g/m^2 oriented in streamwise direction were added to increase bending stiffness of the shells in the cross sectional plane for long-term accuracy. Remaining roughness heights of the wind tunnel model's surface are in the order of 1.5μm RMS measured with a high precision surface quality measuring instrument. The center part of the model was covered with a graphite paint coating to get an electrically conducting surface as end contact for hot-wire measurements (not described herein). Accordingly a small forward facing ramp of about 20 micron height and 5 mm length existed in the center part of the model on both sides. Infrared pictures have shown, that this minimal step has no significant influence on transition position.

In total 62 pressure taps were installed in two oblique rows on suction and pressure side to measure c_p-distributions, employing a PSI type ESP64HD-00 module with full

scale range of 170 mbar. These measurements were used to fine adjust angle-of-attack with boundary-layer traverse systems installed to achieve symmetric c_p's.

2.2. LAYOUT OF SENSOR ARRAY

Target of the investigations was determining the frequency dependent spanwise decay of coherence $g_{p,ij}$ $(w, \mathrm{D}z)$ between two sensors to obtain the spanwise length scale of wall pressure fluctuations:

$$\Lambda_{p,3}(\omega) = \int_0^\infty \gamma_{p,ij}(\omega, \Delta z)\, d\Delta z. \quad (1)$$

The integral over all frequencies is analogous to the two-point correlation index $R_{p,ij}$ (Δz). Traversing of one flush mounted sensor in the airfoil is technically too complicated and too time consuming. So a minimum number of sensors should be employed to cover a large range of length scales. Therefore the spacing of the sensors was arranged according to a potential function $z_i/z_{\max} = a^i/a^N$, $i = 1..N$ in order to get smoothly distributed distances for all sensor pairs. Minimum distance was defined by the sensor width. The finally realized positions were z = [0, 1.85, 5.9, 14.3, 32.0] mm, giving the M unique distances Δz = [1.85, 4.05, 5.9, 8.4, 12.45, 14.3, 17.7, 26.1, 30.15, 32.0] mm. The maximum distance in the array resulted from preliminary measurements. Fig. 2 shows the final flush installation of the sensor array.

A total of five Kulite LQ-062-15-A ultra-miniature pressure sensors with 15 psi full-scale range were flush mounted 4.6 mm upstream of the TE at x/c = 0.989 in a non-equidistant spanwise array on the airfoil (see Fig. 2). Their extremely small thickness of about 0.8 mm allows mounting very close to the trailing edge of wind tunnel models. No

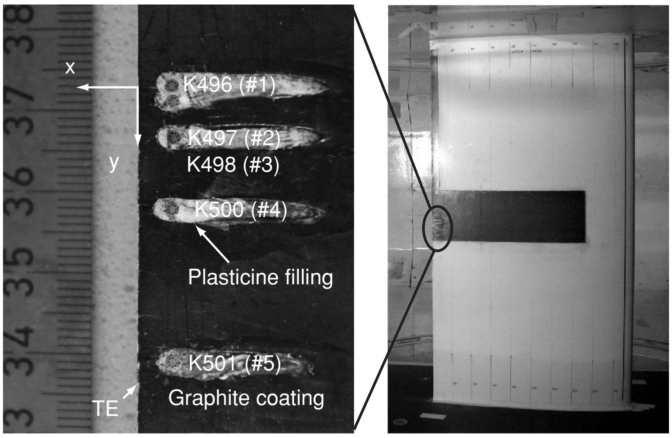

Figure 2: Kulite sensors were integrated in the airfoil using sealing compound and the holes were filled flush with plasticine (left). NACA 0012 airfoil in the test section of the LWT (right).

venting port for static pressure exchange is required, as absolute pressure is sensed. So the sensors were integrated in recesses in the airfoil using Terostat VII sealing compound and the remaining holes were filled flush with plasticine. The sensors were equipped with so called B screens – a circular array of 8 holes of 0.2 mm diameter on a 1.2 mm diameter circle. Their small size shifts the limit of spatial resolution to relatively high wave-numbers. Natural resonance frequency typically is in the order of 200 kHz, allowing a margin of 10 for the frequency range of interest up to 20 kHz. Also the dead volume of the sensors is very small, avoiding Helmholtz resonator effects in the frequency range of interest. Disadvantage is a relatively low sensitivity of the sensors of typ. 6.7 mV/psi at 10 V excitation, which requires strong amplification of the signals for purposes of flow measurements at low airflow speeds.

2.3. SIGNAL CONDITIONING AND DATA ACQUISITION

Keeping electronic noise at a minimum was a target selecting the components of the measurement chain. Bridge amplifiers made by Cosytec based on the INA103 instrument amplifier and the REF102 for providing 10 V excitation were used to operate the Kulite sensors from separate ± 12 V lead gel batteries. The thin sensor cables of about 0.8 m length were twisted to reduce EMC pickup. The AC part of the signals was amplified by 60 dB. A high-pass filter with 190 Hz corner-frequency separates AC and DC part and provides pre-emphasis.

AD-conversion of the amplified signals is accomplished by a 24 bit audio-system RME Hammerfall Multiface DSP at a sampling rate of f_s = 44.1 kHz per channel. The $\Delta\Sigma$ AD converters with 64 times oversampling provide excellent anti-aliasing filtering at half the data rate. The Multiface offers a signal-to-noise ratio (SNR) of 101 dB/106 dBA and cross-talk suppression of > 120 dB. Especially the latter point is important for the correlation measurements, as well as the fact, that the inputs are simultaneously sampled. According to tests maximum phase shifts between the channels remain within 0.5° at the Nyquist frequency. Pressure signals were recorded for 2 min.

2.4. FLOW-FIELD CHARACTERISATION

SPF measurements were performed with clean airfoil and with 2d BL trip strips of 0.36×1.5 mm at $x/c = 0.05$ on suction and pressure side for Reynolds numbers of Re = [0.8 - 1.9]e6, corresponding to Ma = 0.09 - 0.22. Angles-of-attack of $\alpha = [-10 : 2 : 10]°$

were selected, capturing also the LBL-VS noise regime with self-excited oscillations around $\alpha = 6°$. Table 1 gives an overview of the measured data points. Because the airfoil is symmetric, pressure and suction side SPF point spectra can be investigated without remounting the sensors.

To verify values for the displacement thickness δ_1 subsequently used in noise scaling relations, integral BL parameters, Reynolds stresses and fluctuation spectra were obtained from hot-wire measurements (single- and X-wire). A Dantec 55P15 boundary-layer probe with standard 5 μm wire and a DISA 55M10 CTA bridge were employed. The first point of the BL profiles (typically about 25 μm above the surface) is influenced by the cooling of the wall and occasional contacts of the prongs to the conducting surface. Its velocity reading was corrected using the viscous sublayer law and the wall unit determined based on a fit of the Clauser logarithmic law of the wall with $\kappa = 0.41$ and $B = 4.9$ [12].

Table 1. Overview of Kulite measurements on NACA 0012.

dpn	α	trip	*Re*	*t* [°C]	*p* [torr]	ϕ [%]	*r*[kg/m^3]	U_∞ [m/s]	*M*α
measurements after sound absorbing liner installation 25.06.09									
1	0	0	1.5	21.5	703.5	61	1.1020	62.15	0.1800
2	2	0	1.5	21.4	703.4	62	1.1012	62.13	0.1800
3	4	0	1.5	21.3	703.5	62	1.1017	62.10	0.1800
4	6	0	1.5	21.3	703.4	63	1.1015	62.13	0.1798
5	–2	0	1.5	21.4	703.4	61	1.1014	62.14	0.1800
6	–4	0	1.5	21.3	703.4	61	1.1016	62.11	0.1800
7	–6	0	1.5	21.3	703.5	61	1.1019	62.08	0.1800
8	0	1	1.5	21.3	703.3	61	1.1016	62.10	0.1802
9	2	1	1.5	21.4	703.4	60	1.1015	62.12	0.1801
10	4	1	1.5	21.4	703.4	62	1.1012	62.15	0.1803
11	6	1	1.5	21.4	703.4	60	1.1012	62.15	0.1800
12	8	1	1.5	21.4	703.5	60	1.1012	62.16	0.1801
13	10	1	1.5	21.5	703.4	58	1.1013	62.16	0.1805
14	–2	1	1.5	21.5	703.3	59	1.1011	62.17	0.1803
15	–4	1	1.5	21.5	703.4	57	1.1014	62.15	0.1804
16	–6	1	1.5	21.5	703.4	58	1.1011	62.16	0.1804
17	–8	1	1.5	21.5	703.3	58	1.1010	62.19	0.1803
18	–10	1	1.5	21.5	703.3	58	1.1011	62.18	0.1801
19	0	1	1.5	21.4	703.3	59	1.1014	62.13	0.1805
20	0	1	1.7	20.8	698.6	61	1.0960	70.66	0.2062
21	0	1	1.9	20.2	693.3	62	1.0903	79.25	0.2301
23	0	1	1.3	21.6	707.4	64	1.1068	53.60	0.1553
24	0	1	1.0	21.9	712.5	67	1.1133	41.03	0.1189
25	0	1	0.8	22.0	715.3	69	1.1170	32.74	0.0947
measurements after sound absorbing liner installation, improved grounding 28.06.09									
0	0	1	1.448	22.9	709.7	59	1.1053	60.00	0.1739
1	0	1	1.684	22.1	704.5	60	1.1000	70.00	0.2026
2	0	1	1.5	22.1	708.6	64	1.1060	62.10	0.1796
3	0	1	1.7	21.5	704.0	62	1.1012	70.47	0.2044
4	0	1	1.9	20.9	698.7	62	1.0953	79.04	0.2294
5	0	1	1.3	22.6	712.6	61	1.1111	53.53	0.1550
6	0	1	1.0	23.1	717.6	62	1.1166	41.05	0.1188
7	0	1	0.8	23.4	720.1	61	1.1196	32.77	0.0945

In the case picked for detailed discussion later on ($Re = 1.5e6$, $\alpha = 0°$, trip 5%) the following magnitudes are found from the SN-wire measurements at $x/c = 0.990$: $\delta_{99.5} = 9.62$ mm, $\delta_1 = 2.37$ mm, $H_{12} = 1.697$, $Re_{\delta_1} = 4974$. At the measurement position 1 mm downstream of the TE in the wake at $x/c = 1.0025$ some evolution has taken place already to values of $\delta_{99.5} = 10.5$ mm, $\delta_1 = 2.68$ mm, $H_{12} = 1.868$, $Re_{\delta_1} = 5396$. These BL profiles are illustrated in the left plot of Fig. 3. In the wake the BL thickness was obtained for both halves independently and averaged. The perfect symmetry of the wake can be seen looking at the mirrored profiles. The profile in between the pressure sensor position and the wake position, measured at $x/c = 0.9975$, is more close to the upstream one, which indicates that the remaining small bluntness of the TE abruptly increases the displacement thickness in the wake. It is also observed in the streamwise fluctuation velocity profiles in Fig. 3 (rms values in the frequency range 0–15 kHz, upper abszissa), that in the wake the fluctuations increase somewhat.

The obtained δ_1-values as a function of Reynolds number are in good agreement to XFOIL [13], with a trend to slightly higher values, which can be explained by the measurement in the wake. Brooks et al.'s [14] values obtained with a heavy trip, i.e. sandpaper of #60 grit from the LE to $x/c = 0.2$, are significantly larger, because the turbulent boundary layer is additionally thickened on its way over the rough wall. Their 'light trip' values of δ_1 obtained as 60% of the heavy trip

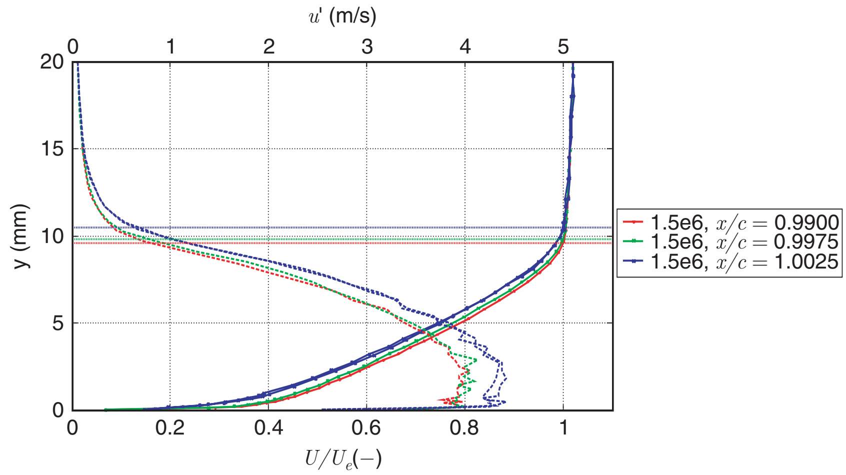

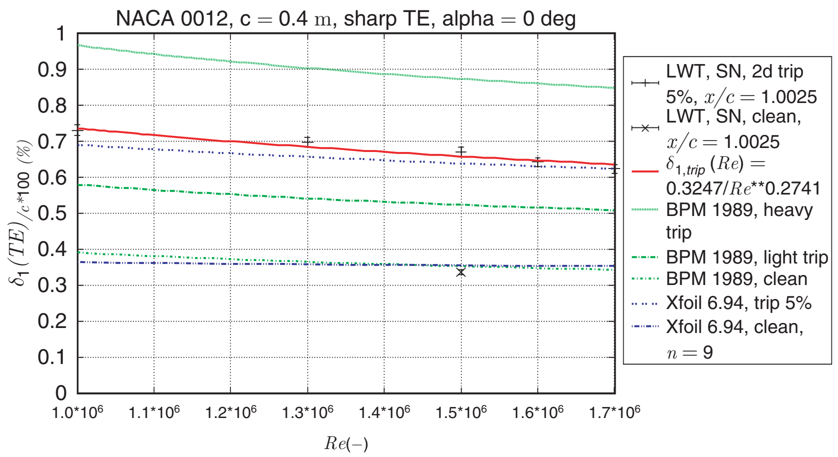

Figure 3: *Measured BL and near wake profiles (left). Comparison of displacement thickness to data from BPM [14] and predictions using Xfoil (right).*

values however are noticably smaller. The clean data match relatively well at Re = 1.5e6.

3. DISCUSSION OF SURFACE PRESSURE DATA

3.1. POINT SPECTRA OF SURFACE PRESSURE FLUCTUATIONS

As a prerequisite for later derivations, the point spectra of wall pressure

$$G_{pp}(\omega) = 2 \cdot \lim_{T\to\infty} \frac{1}{T} E\left[\left|P_w^{(m)}(\omega, T)\right|^2\right] \quad (2)$$

are required, where

$$P_w^{(m)} = \int_0^T p_w^{(m)}(t) \cdot e^{-j\omega \cdot t} dt \quad (3)$$

is the Fourier transform of the mth realization window of surface pressure p_w. Power spectral densities were calculated from the 2 min pressure signals via FFT of approximately n = 1300 blocks of 4096 samples applying a Hanning window. The spectra of sensors #1, 2, 4 were averaged arithmetically, because of slight spectrum contaminations in the low frequency range of sensors #3 and #5, probably due non-perfect flushness of the screen to the surrounding surface. Calibrations with a B&K 4226 multifunction calibrator (modified to get the actuating membrane as close as possible to the sensors due to previous resonance problems) were performed to obtain the frequency response of sensors and amplifier filters. They delivered sensitivity values of about 6.94 mV/psi (average of all sensors at f = 1 kHz).

Fig. 4 shows the spectra of suction and pressure side for angles-of-attack of 0–10° in the tripped case. It can be recognized at a closer look, that at a = 10° the pressure side trip looses its effectiveness and the BL remains laminar up to the TE, as checked via stethoscope. Due to the location of the sensors very close to the TE, then the scattered acoustic field influences the measured surface pressures in a fraction of the frequency range. This will be discussed in more detail in section 4.2.

In Fig. 5 the spectra measured with natural transition are shown. For an AOA of 4° a hump appears in the PS spectrum, because transition location shifts downstream and structures of TS waves remain in the turbulent BL after the transition process. At α = 6° the PS BL remains laminar up to the TE and a feedback loop of radiated sound and disturbances introduced in the BL via receptivity becomes unstable, leading to strong tonal components at certain selected frequencies [15]. These phenomena are not discussed in detail in this paper.

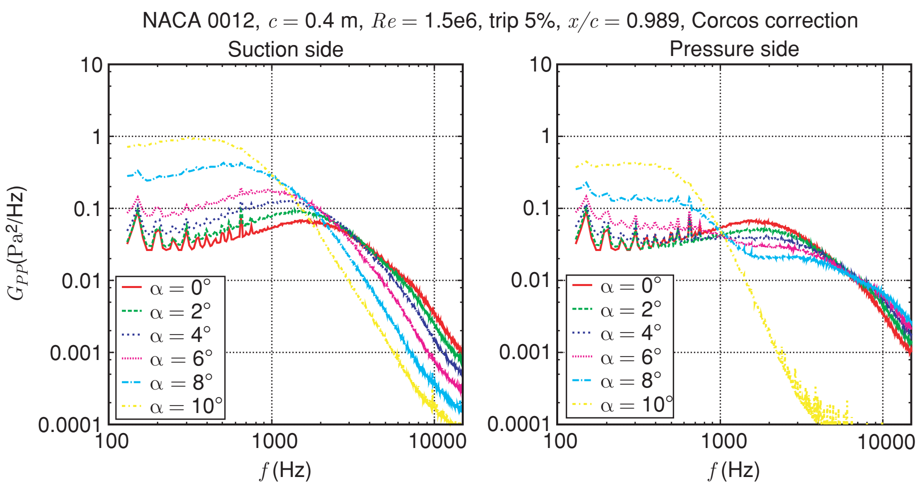

Figure 4: *Measured surface pressure spectra for various angles-of-attack, trip 5%. At α = 10° the pressure side trip loses effectiveness and the spectrum mainly reflects the acoustic influence of the suction side.*

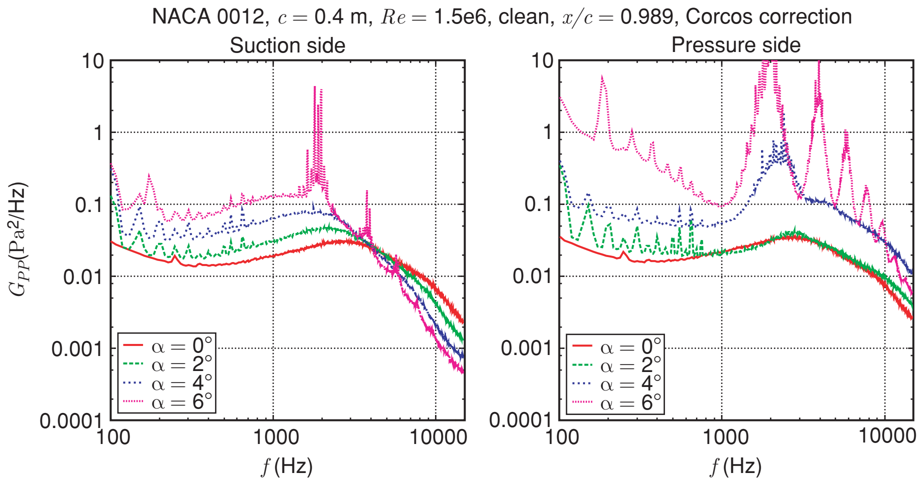

Figure 5: Measured surface pressure spectra for various angles-of-attack, clean.

The Corcos correction function [16, 17] was used to correct the wavenumber averaging effects over the sensor area, using an effective sensor diameter of 1.0 mm. Ten coefficients for a fitted polynomial were used for the tabulated data below $wr/U_c = 4.514$ [18], while five coefficients were used for higher frequencies. It represents only an approximation of the exact response of the B-screen. But due to the mutual connection of the 8 holes by the sensor dead volume the exact response characteristics to the wave-vector spectrum are cumbersome to obtain theoretically, because many parameters like the pressure loss coefficient of the orifices and the shape of the inner structure would have to be known and modeled. Therefore this was not attempted to accomplish. However the exact modeling of this damping is only important at higher frequencies above a few kHz. The simplified criterion proposed by Blake [8], that $fd/U_c < 0.2$, is fulfilled for $f < 8$ kHz with the present mean convective velocity of $U_c \approx 0.7 \cdot U_e \approx 40$ m/s (at the predominantly selected Reynolds number of $Re = 1.5e6$). Therefore in the following the analyses will be confined to $f < 10$ kHz, which is still slightly more than the measurement range obtained on the NACA 0012 with the CPV-method.

The dimensionless size of the transducers defined as $d^+ = d \cdot U_\tau/\nu$ with values ranging from 65–145 in the Re-sweep is not very small compared to

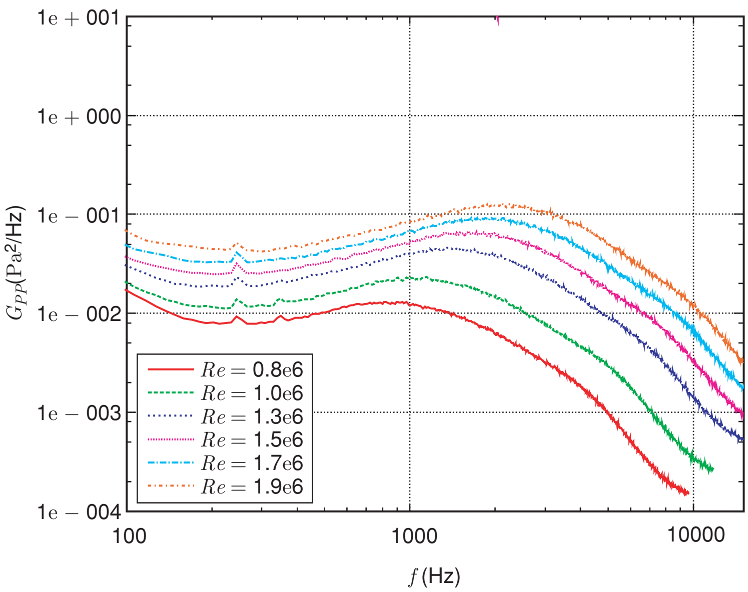

Figure 6: Measured SPF spectra at $\alpha = 0°$ for Reynolds numbers from 0.8–1.9e6.

dedicated measurements with extremely small transducers in thick BLs [19] or at low velocities [20], where $d^+ \approx 20$ were reached. However from a practical viewpoint the sensors can be regarded as relatively small, also considering that the lateral resolution of a standard hot-wire probe with a wire length of 1 mm is not much better.

3.2. VELOCITY SCALING OF SURFACE PRESSURE SPECTRA

To obtain more insight into the validity of the measured SPFs, the scaling of the narrow-band spectra with velocity was considered. Compared to hot-wire measurements one main advantage of pressure transducers is the constancy of sensitivity, so the level of accuracy can be higher. Fig. 7 shows the measured dimensional spectra in the top left, exhibiting the expected amplitude staggering and shift to higher frequencies with increasing Reynolds number. It is also clearly observed, that the electronic noise floor is reached at frequencies of about 8 kHz at the lowest velocity of 30.53 m/s.

In the top right the spectra are normalized with stagnation pressure and displacement thickness according to Blake [8]. A very good match of the rising branch representing the energy containing eddies is observed for non-dimensional frequencies of $\omega\delta_1/U_\infty$ = 0.1–0.4. The spectral maximum is located around 0.3, which is in very good correspondance to acoustic measurement results of the NACA 0012 [8].

The lower left plot shows the spectra scaled on outer variables, normalizing the level by the edge velocity U_e (instead of free-stream velocity, which may be suitable for flat plate experiments), wall shear stress τ_w and displacement thickness δ_1. In the

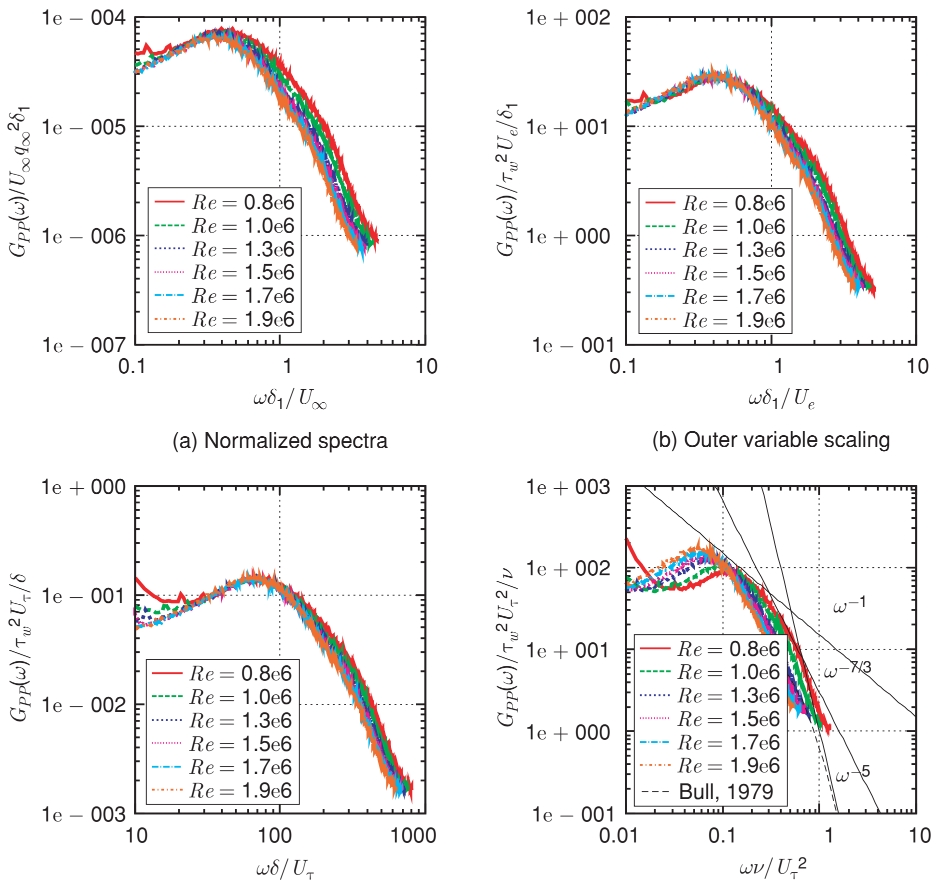

(a) Normalized spectra

(b) Outer variable scaling

(c) Mixed variable scaling

(d) Inner variable scaling

Figure 7: Non-dimensionalized SPF spectra obtained by applying a) normalization with free-stream stagnation pressure and scaled on b) outer, c) mixed and d) inner variables.

average the matching is slightly better, reducing a bit the spread at high-frequencies at the price of a worse agreement in the energy containing range. Because at the position of the pressure transducers the BL profile was measured for only $Re = 1.5e6$, the BL parameters were obtained from Xfoil. That this is a justified approach for this simple flow case (without separation) can be seen in Fig. 3 in section 2.4.

In the lower right of Fig. 7 inner variables are used for scaling. The high-frequency range should now match, but it doesn't do particularly good. However it must be said, that also in other investigations (on flat plate BLs) [21, 19] no particularly good match in inner variables was observed. The sensor characteristics might influence the measured spectra in the high-frequency range. At least the non-dimensional frequency of the change of spectral roll-off from w^{-1} to w^{-5} matches Bull's relation for high-frequency damping quite well.

Just for completeness it is mentioned that the best fit of the SPF power density spectra is obtained with a constant reference length for the Strouhal number fL/U and power law scaling of spectral energy with $U^{2.5}$.

To conclude – in the frequency region around the spectral maximum little uncertainty is present in the measured G_{pp}, while at high frequencies the amplitudes could be biased somewhat due to spatial resolution effects not being corrected exactly.

3.3. COMPARISON OF POINT SPECTRA TO THEORETICAL MODELS

As an intermediate step, the point spectra lend themselves for comparison to and validation of aeroacoustic prediction codes, because few data transformations are involved in the experiment and on the theoretical side no utilization of a relation for far-field noise radiation is necessary.

In the IAGnoise code [22] several methods can be selected for predicting TBL-TE noise. The main difference is evaluation of the aerodynamic properties, i.e. the BL profile, Reynolds stresses and length scales. The most simple method Xnoise uses XFOIL [13] to predict integral TBL parameters. But the BL profiles derived from these are often not very accurate, which leads to unreasonable behaviour also in the prediction of TE noise. A more refined approach established in IAGnoise is the XEnoise method, using the finite difference BL scheme EDDYBL [23] to predict BL profiles and turbulent fluctuations. The computationally most expensive approach, employing the RANS code FLOWer for prediction of the turbulence quantities, is called Rnoise [24, 25].

Facing the wall pressure fluctuations predicted with the Rnoise model based on the $x/c = 0.99$ profiles to the Kulite measurements for angles of attack of 0–6° in Fig. 8 it can be noticed, that the qualitative agreement of shape, level and staggering is very good. At low frequencies facility noise and 50 Hz harmonics influenced the measured spectra significantly, leading to the observed differences. Increasing AOA, the suction side spectra (left) increase in level and maxima shift to lower frequencies, while on the pressure side (right) amplitudes drop and maxima shift to higher frequencies as expected. The frequency of a common crossover of the spectra is slightly higher in the measurements than in the predictions. Anyhow, agreement of the maximum positions is very good after an adaptation of the modeling of the wave-number of the most energetic eddies κ_e, which is based on the high frequency asymptote of Kolmogorov and von Kármán spectrum.

In the process of attributing deviations either to the aerodynamic code or the theoretical formulation for the surface pressure spectra, the measured BL quantities at $x/c = 1.0025$ were used as an input to the prediction model. BL profile, fluctuations and

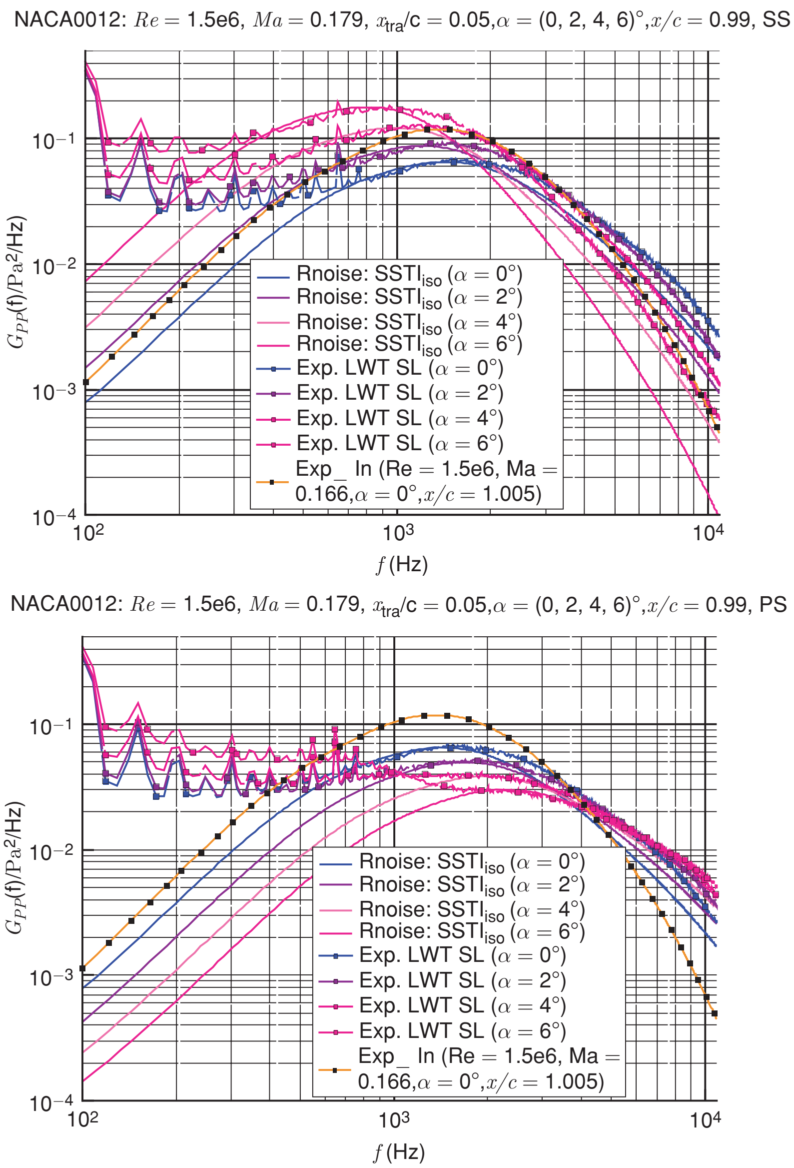

Figure 8: *Comparison of measured and predicted SPF spectra for various angles-of-attack, trip 5%. Left plot shows suction side, right plot pressure side.*

length scales had been measured by X-wire probes in the near wake of the airfoil [25]. The measurements were performed in the wake, because with the X-wires measurements over the wall are not possible close enough to the surface.

Agreement of the spectrum for zero AOA obtained from feeding the measured quantities into the prediction code is quite good concerning peak level and location of the maximum, see Fig. 8, curve "Exp_in". However the shape of the "Exp_in" G_{pp} spectrum rather corresponds best to the 4° case. This can probably be attributed to the streamwise evolution of the BL. As seen in section 2.4 the BL profile at the hot-wire position at $x/c = 1.0025$ has thickened about 10% compared to the one at $x/c = 0.99$, so an increase of levels at frequencies below the maximum is expected. Also a decrease at high frequencies is likely due to the smaller gradient dU/dy in the lower part of the wake profile. However these changes are not expected in the magnitude seen in Fig. 8. Rather about 10% of peak spectral energy reduction are anticipated from the normalization according to section 3.2.

Anyhow it is concluded, that the good agreement between measured and theoretical point frequency spectra confirms validity of the prediction approach for the wavenumber-frequency spectrum. Performing these comparisons, also the reason for a long-observed offset of far-field noise spectra predicted by the original TNO model [26] compared to absolute sound-pressure measurements in the order of –8 dB could be found. For the present investigations all the computations have been conducted by the modified TNO model.

3.4. SPANWISE LENGTH SCALES OF SURFACE PRESSURE FLUCTUATIONS

From e.g. [27, 8] the behaviour of pressure fluctuations under turbulent boundary layers is relatively well known.

Spanwise homogeneity of the BL parameters provided, two methods for obtaining approximations for the integral (1) were applied:

i) using the trapezoidal rule within the given Δz-limits of the array, obtaining $\Lambda_{p,3}$ as $\sum_{k=1}^{(M-1)} (\gamma_{p,k} + \gamma_{p,k+1}) \cdot \Delta z_k/2$ over the monotonically sorted separations, where a linear extension to $\gamma_p(\Delta z = 0) = 1$ is performed, or

ii) via curve-fitting an exponential decay function $\gamma_p(w, \Delta z) = \exp(-K\Delta z)$ to the measured coherence-separation pairs, analogous to two-point correlations of velocity fluctuations. In this case $\Lambda_{p,3} = 1/K$.[2] Very good agreement of this exponential coherence decay model to the measurements was observed over a large frequency range. Accordingly at $\alpha = 0°$ within $f = 200 – 2000$ Hz, the most interesting frequency range for TE noise acoustics for the prevailing flow case, practically no difference exists between both approaches (Fig. 9 lower right). For lower frequencies coherence $\gamma_{p,ij}$ does not decay to zero within the size limit of the array. This is also observable in the 2d-plots of coherence in Fig. 10. At larger AOAs on the suction side the "clipping" of coherence happens already at higher frequencies, so that the $\Lambda_{p,3}$ values from the fitting approach generally provide better estimates. For thin BLs the length scales become quite small and low coherence values remain at large separation distances, due to the statistic properties. The integration of these small remaining values increases $\Lambda_{p,3}$, so again a reason exists to choose the fitting approach. A more refined function would include the parabolic flattening of the coherence peak at zero separation distance caused by the bandwidth limitation of the signals. But in the frame of the investigations described herein this small possible increase of accuracy was not regarded as crucial for the conclusion to be drawn.

The $\Lambda_{p,3}$ values obtained for different *Re* scale very well on a Strouhal number formed with displacement thickness δ_1 like the SPF spectra (see Fig. 11). In the high-frequency branch a $1/f$ proportionality has been observed, which is however lost below the frequency of the spectral maximum.

At low frequencies the length scales show some spiky outliers at fixed frequencies, which may be caused by higher harmonics of 50 Hz humm. Also the possibility of coherence biases due to the acceleration response of the pressure sensors to structural vibrations of the wind tunnel model was considered as a cause. This was assessed by Laser Scanning Vibrometer measurements of the wall normal surface velocity in previous investigations on a similar N0012_04a

[2]It could be mentioned here, that spatially assigning the coherence value to the middle of the sensor pair is straight-forward, but is some extension of the explanations in [25].

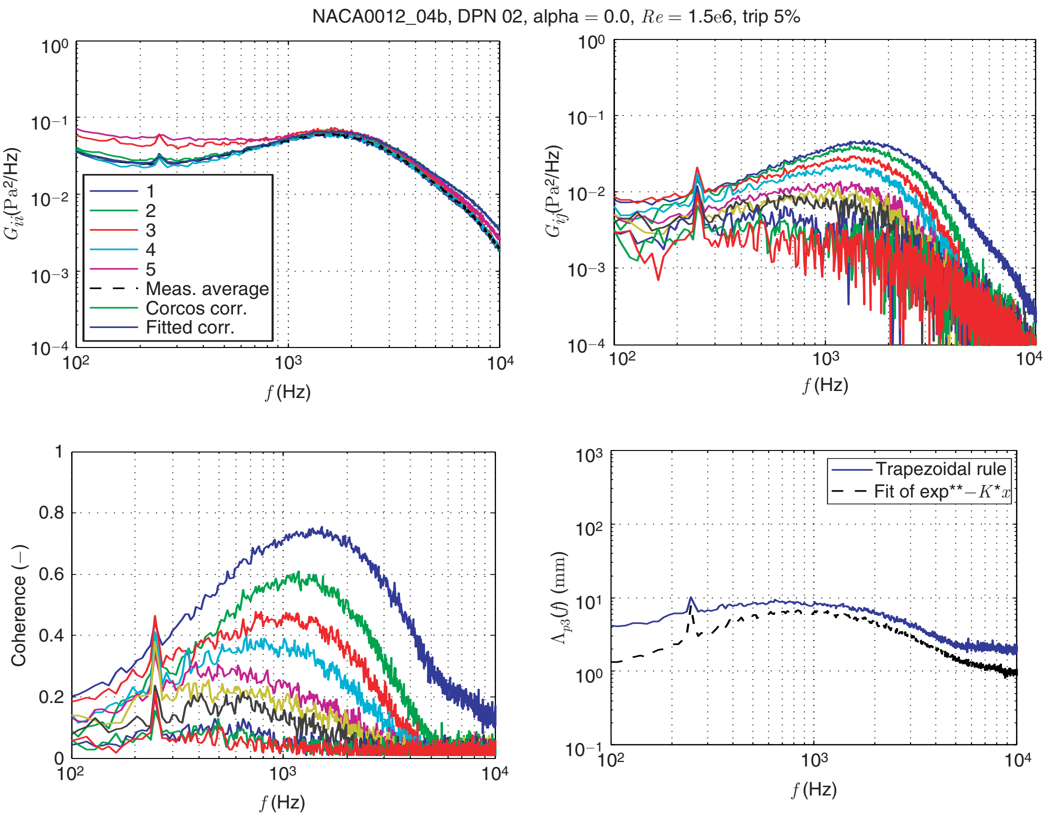

Figure 9: *Auto and cross power density spectra, coherence and spanwise length scales of surface pressures as measured on the NACA 0012.*

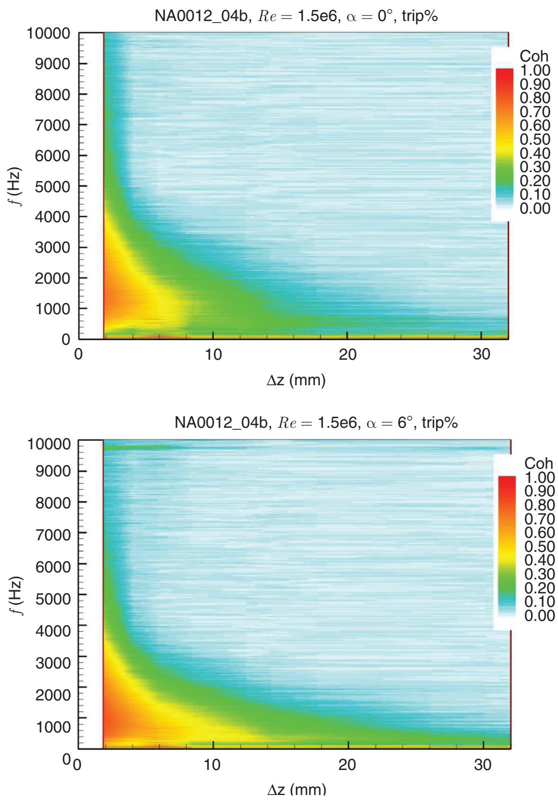

Figure 10: *Coherence vs. spanwise separation and frequency measured on the tripped NACA 0012 for angles-of-attack of 0 and 6°.*

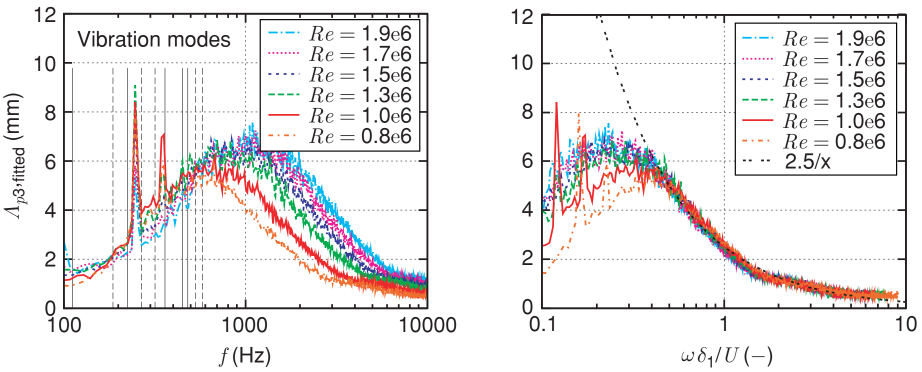

Figure 11: *Measured $\Lambda_{p,3}(w)$ values for various Reynolds numbers (left). The scaling on a Strouhal number formed with displacement thickness (right) shows good collapse of the data for non-dimensional frequencies between 0.3 and 2.*

wind tunnel model made from solid glass fiber laminates. It was found that the airfoil responds to the stochastic forcing in its mode shapes within narrow frequency bands. Some of the lower eigenfrequencies are plotted in Fig. 11. Those which have significant deflections at the sensor position are shown in solid lines. The N0012_04b model reinforced with some UD carbon-fiber will have slightly raised eigenfrequencies due to higher stiffness to mass ratio. In view of this, it could be possible, that the two prominent peaks at 250 and 350 Hz are caused by sensor vibrations. However the pressure sensor outputs calculated from the measured wall vibrations with the given acceleration sensitivity of the Kulites are significantly lower than those obtained in the BL. So it seems that other sources for these disturbing peaks exist and vibrations do not influence coherence significantly.

4. ESTIMATIONS OF FAR-FIELD NOISE

4.1. DETERMINATION OF RADIATED FAR-FIELD NOISE LEVELS

The challenge of obtaining radiated far-field noise from wall pressure fluctuations has been of interest since a long time. As mentioned introductorily, many investigations are described in available literature dealing with ways to determine the sound pressure spectrum in the far-field $G_{p,ff}$ from point spectra of wall pressure fluctuations G_{pp}.

Three ways for the so called scattered surface pressure prediction (SSPP) were investigated concerning their applicability at the example of the NACA 0012. The key point in all approaches is, that $G_{p,ff}$ is assumed to be proportional to the spanwise length scales $\Lambda_{p,3}$.

The empirical relation given by Brooks & Hodgson [7], based on Howe's [28] formulation, for the case $\varphi = 90°$

$$G_{p,ff}(\omega,\ r) \approx (1/2\pi^2 r^2)(U_c/c_0)/ \\ /(1-U_c/c_0)L_{ref}\Lambda_{p,3}(\omega)\cdot G_{pp}(\omega) \tag{4}$$

is one possible way to arrive at the desired estimation of far-field noise. Here it had been assumed by Brooks that the pressure fluctuations at the TE are half as large as those upstream of the TE (Kutta condition).

Blake's [8] formulation (p. 788)

$$G_{p,ff}(\omega,r) \approx (1/8\pi^2 r^2) \\ L_{ref} Ma_c \Lambda_{p,3}(\omega)\cdot G_{pp}(\omega) \tag{5}$$

differs only slightly in terms of the effect of convective Mach number $Ma_c = U_c/c_0$, but leads to significantly lower values due to the factor 1/8 instead of 1/2.[3]

From the narrow band spectrum $G_{p,ff}$ obtained from the SPF PSDs then third-octave band spectra are calculated for L_{ref} = 1 m, r = 1 m and transformed to sound pressure levels $L_p = 10 \cdot \lg(G_{p,ff} \cdot df/4 \cdot 10^{-10})$, having the unit [dB/m].

Blake's formulation for third-octave band levels (p. 791)

$$L_{p,ff}(r,f,\Delta f) = L_{surf}(x_{TE},f,\Delta f) + 10\cdot\lg(U_c/c_0) + 10\cdot\lg(L_{ref}\Lambda_{p,3}\,/\,r^2) - 10\cdot\lg(\zeta(x_{TE})) - 20 \quad (6)$$

is practically equivalent to eqn. (5), just the offset is generously rounded. Herein $\zeta(x_{TE})$ is a factor taking into account the distance of the sensors from the TE.

Contributions of both airfoil side contributions are summed energetically. This of course only applies to broadband noise cases without mutual coherence of the pressures of both sides.[4]

In Fig. 12 the SSPP values for α = 0° obtained by equations 4–6 are compared to CPV-measurements and numerical predictions. As expected the values of Brooks are shifted by about +6 dB compared to the values of Blake, which is explainable by the different proportionality factors. The CPV-results are located in between both formulations.

4.2. INFLUENCE OF SCATTERED PRESSURE ON UPSTREAM SURFACE PRESSURE

As mentioned in section 3.1, the sound radiated from the trailing-edge has an upstream influence on the pressure sensors. In our case of proximity of the TE we can show, that in the mid-frequency range the acoustic disturbances come from the TE, even without measuring their convective velocity.

The first strong sign is, that a change in AOA alters the spectra in frequency ranges dominated by acoustic

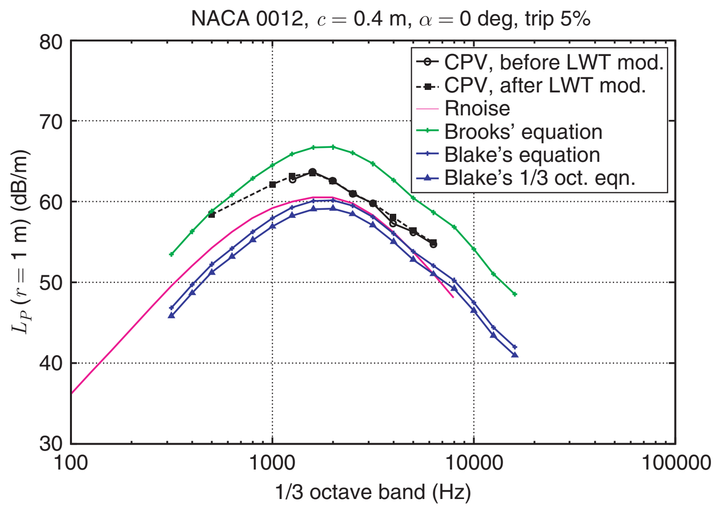

Figure 12: Comparison of third-octave SPLs obtained from the pressure fluctuations by equations 4–6 to those measured by the CPV-method (black) and predicted by Rnoise (magenta).

[3]When the incident SPF spectrum is introduced as one-sided, then also the result constitutes a one-sided spectrum. Anyhow it is believed, that this factor of 4 difference is attributable to different conventions in the definition of spectra between the two authors. When Blake's results would actually represent two-sided spectra, which is also assumed by other researchers [29], the values would have to be shifted 3 dB up. This would indeed improve the comparison substantially.

[4]In cases with tonal noise it would probably fail, because the coherence of the two sides requires a phase-correct adding of amplitudes. However here it helps, that at low Mach numbers the scattered sound pressures are much below the hydrodynamic pressures, so with a reasonable sensor-TE distance these amplitude biases may not be dramatic.

contributions of the other surface. This could for example be seen in the α-sweeps in Fig. 4, where e.g. for the PS (right) at $\alpha = 8.0°$ a hump develops below $f = 1200$ Hz with the maximum at about 700 Hz, roughly where the maximum of the pressure fluctuations on the SS is located (left). Also vice versa the PS influences the SS at high frequencies.

It should be avoided that the measured SPFs are strongly influenced by TE acoustics, because predicted far-field spectra can then be biased by multiple effects. Besides the primary effect of an increase of G_{pp}, also, as a secondary effect, the length scales $\Lambda_{p,3}$ can be artificially increased and the summation of airfoil side contributions biases the total spectrum.

So selecting the streamwise position of the sensors is governed by several compromises to make. On the one hand a position as close to the TE as possible is desired from the viewpoint of similarity of the spectral properties to those at the TE in the general case of streamwise non-constant BL development on an airfoil. However, the acoustic fraction of the wave-number spectra gets higher energy the closer the sensors come to the TE.

To detect the influenced parts of the spectra more precisely, a more quantitative criterion needs to be found. Interestingly, this also offers a way to check the proportionality of sound radiation to $\Lambda_{p,3}$.

If $\Lambda_{p,3}$ is a proportionality factor for the radiated sound pressure and the sensors pick up acoustic pressure fluctuations from the TE, then the ratio

$$\chi_{ss} = \frac{G_{pp,ss} \cdot \Lambda_{p,3,ss}}{G_{pp,ps}} \qquad (7)$$

is constant when the suction side acoustically influences the pressure side and

$$\chi_{ps} = \frac{G_{pp,ps} \cdot \Lambda_{p,3,ps}}{G_{pp,ss}} \qquad (8)$$

is constant, when the PS influences the SS.

In Fig. 13 indeed one can see, that a plateau of c_{ss} forms from 500–1200 Hz at $\alpha = 4°$ and 200–1200 Hz at $\alpha = 8°$, which confirms the above assumption. At the lower AOA the tunnel background noise still becomes significant at the very low frequencies

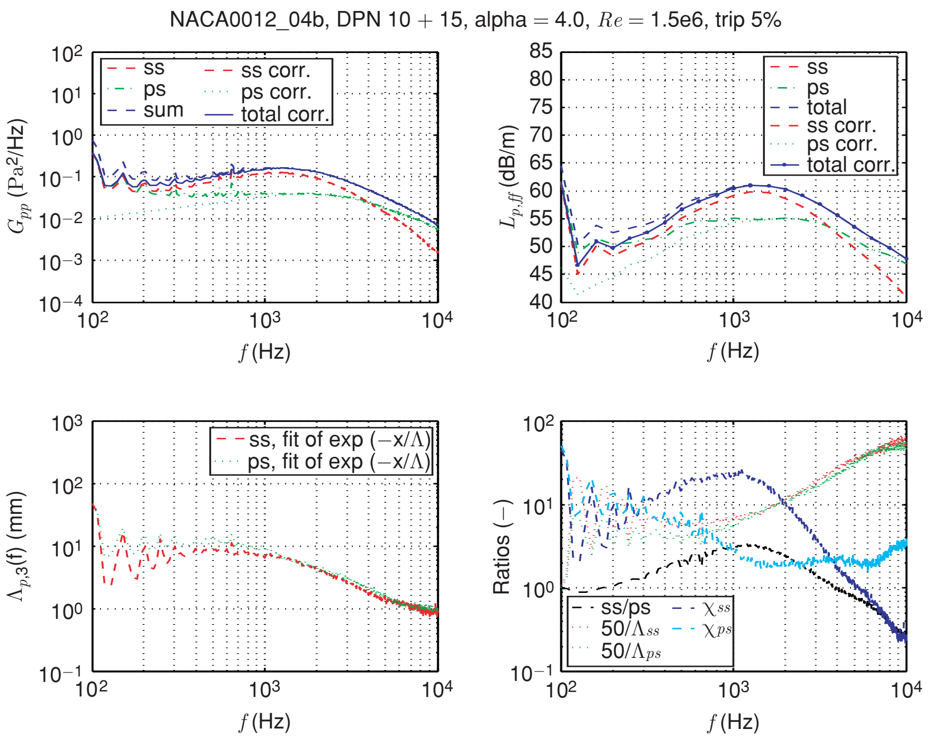

Figure 13: (Continued)

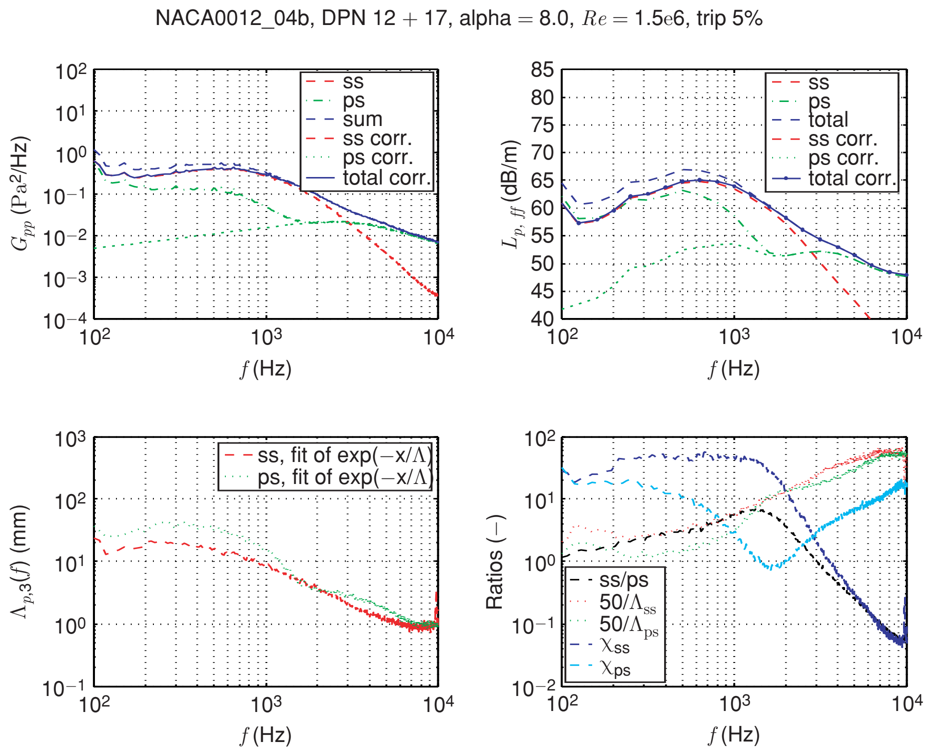

Figure 13: *Measured surface pressure PSDs of PS and SS (upper left), third-octave spectra of estimated far-field noise decomposed in PS and SS (upper right) and SPF length scales (lower left). The upstream influence of scattered pressure can be identified from the ratio of SS and PS spectra (lower right plot, black). At the frequency where the contribution becomes significant (< 1.2 kHz), the slope of the ratio changes sign and the curve quite well reflects the inverse $\Lambda_{p,3}$ development of the emitting suction side.*

and distorts the curve. For the higher AOAs, saturation of c_{ss} to a constant value around 50 is observed, indicating the amplitude decay of acoustic waves over the distance of radiation.

When the c-values exceed a certain threshold χ_{crit}, the respective side should not be taken into account for the power summing. To more appropriately correct the primary influence of acoustic contributions on the pressure fluctuations, the spectra are replaced by an extrapolation with $p \sim f^2$ for $f < f(\chi_{crit})$ (compare Fig. 13 upper left plot).

The PS hardly influences the SS in the present case, because at the involved high fre- quencies the $\Lambda_{p,3}$-values are very small – accordingly sound radiation is not so efficient. For zero AOA with equal SPFs and sound radiation from both sides all this is not a problem, because the amplitude decay of scattered pressures provides enough damping at the selected position 4.6 mm upstream of the edge.

4.3. VELOCITY SCALING OF PREDICTED FAR-FIELD NOISE

The velocity scaling of narrow-band SPF spectra was already considered in section 3.2. Now the variation of far-field noise third-octave spectra predicted by the SSPP method shall be investigated, because suitable relations are well known from previous trailing-edge noise measurements and allow a validation of the proposed method. In Fig. 14 (a) the third-octave spectra obtained for Reynolds numbers of 0.8 to 1.9 million are compared on a dimensional basis to elliptic mirror measurements from the Aeroacoustic Wind Tunnel Braunschweig (AWB) on a NACA 0012 airfoil of the same chord ([30], zigzag trip at $x/c = 0.1$), as well as CPV results obtained after the recent

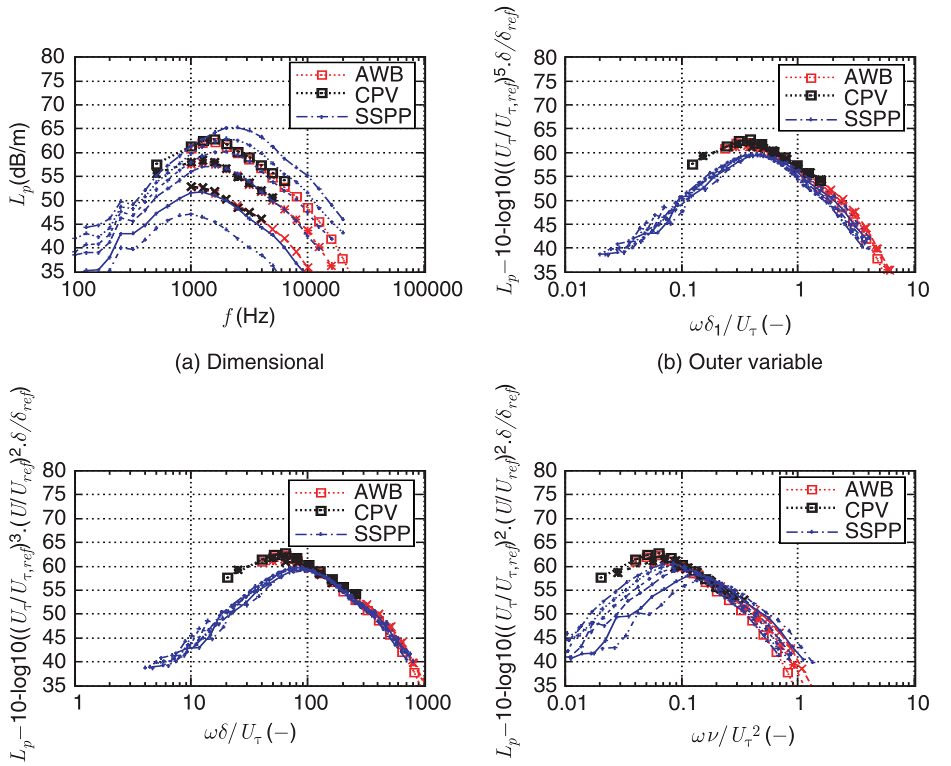

(a) Dimensional (b) Outer variable (c) Mixed variable (d) Inner variable

Figure 14: Comparison of dimensional (a) and SSPP spectra scaled on different variables (b–d) to acoustic NACA 0012 measurements in LWT and AWB.

sound absorbing lining installation in the LWT. AWB and LWT results agree almost perfectly. Different test velocities are responsible for the scattering of the SSPP curves around the direct acoustic results.

In plot (b) non-dimensional spectra are compared on a basis of outer variable scaling typically proposed for matching the maxima of TE noise spectra. Identical BL parameters for LWT and AWB have been assumed and all spectra were referenced to a velocity of $U_{ref} = 60$ m/s. Now the SSPP results compare very well with the two other measurement methods, being only slightly shifted to lower levels (remember the different factors in section 4.1). The general trend appears again, that for decreasing Reynolds numbers the high-frequency branches seem shifted to slightly higher levels, while the low-frequency branches collapse. This was already noticed for the surface pressure measurements (section 3.2). It is nice to see, that in both AWB and SSPP spectra the transition to stronger decay (overlap to inner region) happens at more or less the same non-dimensional frequency $w\delta_1/U_\infty \approx 2$. With the chosen acquisition time of 7 min the CPV method was not able to resolve this frequency region due to electronic noise.

Plot (c) of Fig. 14 shows spectra in mixed variable scaling [31]. The maxima of the individual measurements are matched better and the decaying branches of the spectra collapse perfectly.

Inner variable scaling (d) does not lead to a good collapse neither for the AWB measurements nor the SSPP data. This was already observed for the SPF spectra in section 3.2. The “knees” around $w\nu/U_t^2 \approx 0.8$ were in better agreement with the mixed variable scaling. Whether this reflects shortcomings of the spatial resolution correction at high wavenumbers, small coherence biases due signal-to-noise ratio of the sensors or that the inner variable scaling is not appropriate in this form still is not completely cleared yet and further investigations would be welcome.

4.4. COMPARISONS OF FAR-FIELD NOISE PREDICTIONS TO ACOUSTIC MEASUREMENTS

The estimates of far-field noise from surface pressure fluctuations according to eqn. (5) are compared to acoustic measurements by the CPV method. In Fig. 15 results of the NACA 0012 SPF measurements are shown in blue for angles-of-attack between 0 and 10°, plotting third-octave band spectra of sound pressure levels versus center frequency. The total power summed spectra are combined from the individual pressure and suction side contributions. As accustomed, the SPLs are referenced to L_{ref} = 1 m and an observer at a distance of r = 1 m and φ = 90°, accordingly having the unit dB/m.

For comparison also semi-empirical predictions with the Rnoise code [32, 22] are plotted, indicating the expected shifting of PS and SS contributions with variation of AOA. They agree quite favourably with the individual contributions obtained with the SSPP

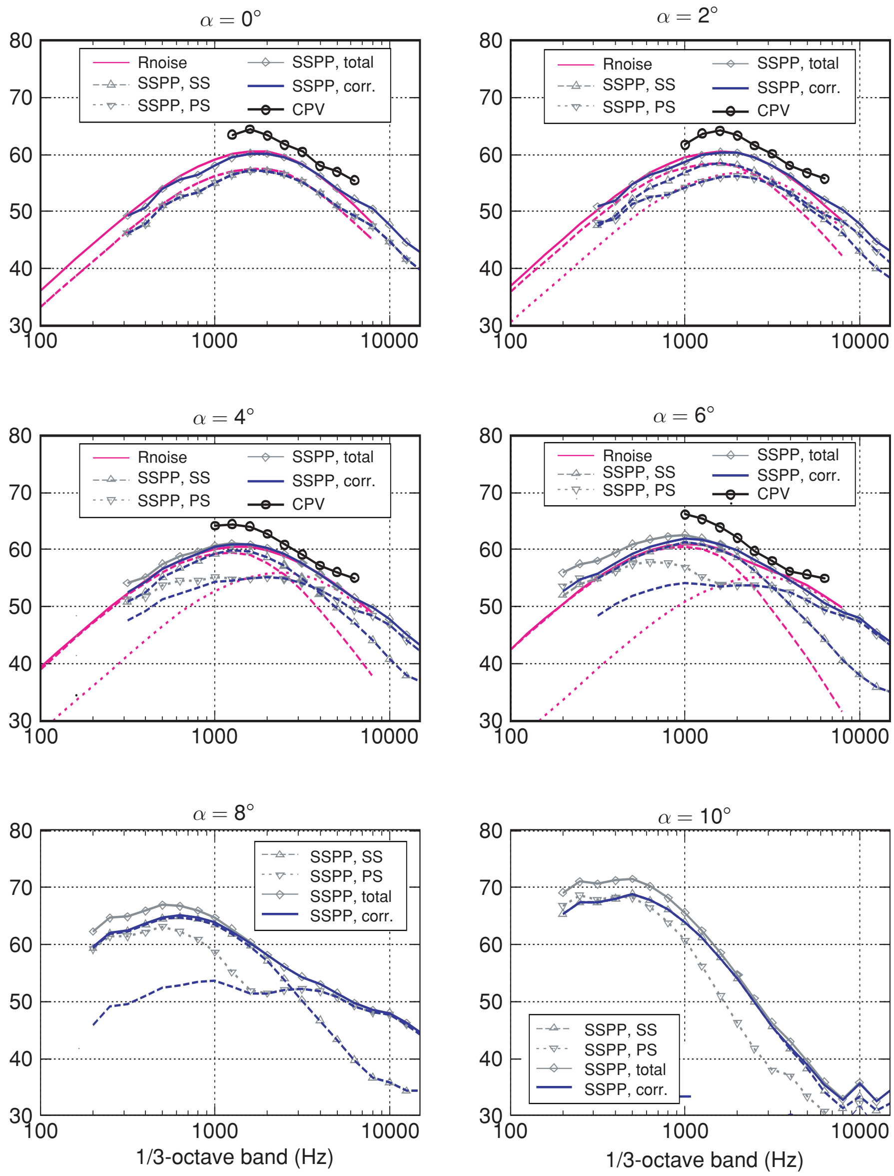

Figure 15: Comparison of CPV-measured SPLs on NA0012_04b (black) to those obtained from the pressure fluctuations (blue) and predicted by Rnoise (magenta). The gray curves represent the results without removing the acoustic contaminations in Gpp.

method. For AOAs above 6° no Rnoise results could be obtained due to convergence problems. It should be mentioned again, that at 10° the pressure side BL trip lost effectiveness in reality in contrast to the calculation. So the PS curve only reflects the SS contribution due to pick-up of sound of the opposite airfoil side and the characteristic knee is missing.

In general, agreement of magnitude and spectral shape to the CPV measurements is very good in the high-frequency part of the spectra, dominated by the overlap region of the boundary layer. The SSPP method covers a significantly larger frequency range here, exceeding 10 kHz easily due to good signal-to-noise ratio. The roll-off on the right side of the maximum starts a bit more gradual, such that the peak appears a bit more rounded. Also, the CPV measurements seem to develop a slightly stronger mid-frequency kink for higher angles of attack.

In the frequency range around 500–600 Hz there is a minimal hump in the SSPP spectra. These are effects of higher harmonics of 50 Hz humm, as could be shown in later measurements, where the battery powered Kulite amplifiers had been grounded to the measurement equipment (compare the narrow-band spectra in Fig. 6). Unfortunately these new measurements could only be performed for zero degree AOA.

On the low-frequency side there are hardly enough third-octave bands available from the CPV measurements for a serious comparison. The CPV spectra, measured before the LWT absorbing lining modification, are processed with a background noise correction [33]. This mainly compensates most of the amplitude loss at the lower end of the spectra, but does not increase bandwidth. The numerical predictions with Rnoise show a slope at low frequencies which is very similar to the SSPP measurements, confirming the applicability of the approach. This makes it possible to conclude, that an extension of the measurement range at low frequencies can be obtained with the SSPP method, which in fact was the particular target of development.

The condition that the spectrum is evaluated "well upstream" of the TE, so that $x_{TE}w/U_c > 1$, is fulfilled for frequencies above approximately 1.3 kHz in the prevailing case. In this case $\zeta(x_{TE}) = 1$. For $x_{TE}w/U_c$ approaching zero, Blake suggests that $\zeta(x_{TE}) \rightarrow 1/4$. This means, that the levels from the surface pressures predicted by eqn. (5) could be too low for lower frequencies. Indeed the comparison to the measured and numerically predicted far-field noise spectra in Fig. 14 and 15 shows the maxima of the SSPP spectra shifted slightly to higher frequencies. Experience about the transition of the $\zeta(x_{TE})$-curve to 1/4 is still too scarce for including this factor in the calculation of third-octave spectra, however.

5. CONCLUSIONS

An efficient method to obtain estimates of radiated sound pressures from turbulent boundary-layers on two-dimensional airfoil sections in low-turbulence flow based on surface pressure measurements was evaluated and validated on a NACA 0012 airfoil section. The so called scattered surface pressure prediction (SSPP) method distinguishes itself from common acoustic measurement methods for noisy wind tunnels by shorter measurement times and larger frequency range. It is insensitive to background noise and free-stream turbulence levels in the wind tunnel. This is due to the fact that hydrodynamic quantities are acquired with very good signal-to-noise ratio.

For the investigated broadband TBL-TE regimes on a tripped airfoil, far-field spectra predicted from surface pressures compare favourably with predictions by the IAGnoise code ("Rnoise" mode), the CPV-method and those obtained by an elliptic mirror in an aeroacoustic facility (AWB). Deviations in absolute levels are within a few dB and frequencies of the maxima match well. The low-frequency limit of TE noise spectra obtained on a $c = 0.4$ m chord NACA 0012 has been reduced to approximately one third of the benchmark measurements, allowing to capture a large portion of the branch left of the maximum.

A specific advantage of the SSPP method is the possibility to separately measure the contributions of pressure and suction side BLs to the radiated far-field noise. It is free of the influence of parasitic corner sources possibly present at the intersection of wind-tunnel wall and airfoil section. Installed in a rotating wind turbine blade it would allow insights about source characteristics without the influence of convective, Doppler and atmospheric propagation effects.

Concerning accuracy, small differences between pressure spectra at sensor position and TE, caused by streamwise gradients of BL parameters, are to be achieved. However it is not necessarily beneficial to place the sensors very close to the TE, because of acoustic cross-talk effects from the other airfoil side when the BLs are very dissimilar. If the absolute distance from the TE is large enough, the contaminated parts of the spectra can be omitted or replaced by an extrapolation. It was shown, that the spanwise length scales of pressure fluctuations indeed are a proportionality factor for the sound radiation. This is very helpful to locate the frequency regions of contamination by a criterion based on the ratio of PS and SS spectra.

The SSPP approach was tested for a sharp TE geometry until now. Other radiation efficiency factors for blunt TEs (squared or rounded) still need to be investigated. The theory derived in [34] might be helpful in this.

To fully establish the method as a measurement technique, the insights into the source Green's function defining radiation directivity, which were gained in theoretical research like [35, 36, 37], still can be applied. Precision at high frequencies is relying on the availability of precise corrections for sensor spatial resolution. At low frequencies, where the sensors are not "well-upstream" of the TE related to the eddy size, further investigations about the development of the z-factor are necessary. So up to now, the SSPP method is not to be considered as a replacement, but rather a supplement of prevailing measurement techniques.

REFERENCES

[1] Würz, W., Guidati, S., Herrig, A., Lutz, T., and Wagner, S., "Measurement of Trailing Edge Noise by a Coherent Particle Velocimetry Method," Int. Conference on Methods of Aerophysical Research ICMAR, Novosibirsk, 28.06.–02.07. 2004.

[2] Herrig, A., Würz, W., Lutz, T., and Krämer, E., "Trailing-Edge Noise Measurements Using a Hot-Wire Based Coherent Particle Velocity Method," 24th Applied Aerodynamics Conference, San Francisco, California, 5–8 June 2006, AIAA 2006–3876.

[3] Lutz, T., Herrig, A., Würz, W., Kamruzzaman, M., and Krämer, E., "Design and Wind-Tunnel Verification of Low-Noise Airfoils for Wind Turbines," 24th Applied Aerodynamics Conference, San Francisco, California, 5–8 June 2006, AIAA 2006–3322.

[4] Herrig, A., Würz, W., Lutz, T., Krämer, E., and Wagner, S., "Trailing-Edge Noise Measurements of a NACA 0012 Airfoil using the Coherent Particle Velocity Method," Int. Conference on Methods of Aerophysical Research ICMAR, Novosibirsk, 05.02.–10.02. 2007.

[5] Brooks, T. F. and Humphreys, W. M., "A deconvolution approach for the mapping of acoustic sources (DAMAS) determined from phased microphone arrays," *Journal of Sound and Vibration*, Vol. 294, No. 4–5, 2006, pp. 856–879.

[6] Sijtsma, P., "CLEAN Based on Spatial Source Coherence," 13th AIAA/CEAS Aeroacoustics Conference, Rome, 21–23 May 2007, AIAA 2007–3436.

[7] Brooks, T. F. and Hodgson, T., "Trailing Edge Noise Predictions from Measured Surface Pressures," *Journal of Sound and Vibration*, Vol. 78, No. 1, 1981, pp. 69–117.

[8] Blake, W. K., *Mechanics of Flow-Induced Sound and Vibration*, Vol. 2, Complex Flow-Structure Interactions of *Applied Mathematics and Mechanics*, Academic Press, Inc., Orlando, Florida 32887, 17th ed., 1986.

[9] Wortmann, F. X. and Althaus, D., "Der Laminarwindkanal des Instituts für Aero-und Gasdynamik an der Technischen Hochschule Stuttgart," *Zeitschrift für Flugwissenschaften*, Vol. 12, No. 4, April 1964, pp. 129–134.

[10] Plogmann, B., "Background Noise Measurements in the Laminar Wind Tunnel," Tech. rep., University of Stuttgart, Institute of Aerodynamics and Gas Dynamics, Jan. 2010.

[11] Pott-Pollenske, M. and Delfs, J., "Enhanced Capabilities of the Aeroacoustic Wind Tunnel Braunschweig," 14th AIAA/CEAS Aeroacoustics Conference (29th AIAA Aeroacoustics Conference), Vancouver, Canada, 5–7 May 2008, AIAA-2008–2910.

[12] Klewicki, J. C., Saric, W. S., Marusic, I., and Eaton, J. K., "Wall-Bounded Flows," *Springer Handbook of Experimental Fluid Mechanics*, edited by C. Tropea, A. L. Yarin, and J. F. Foss, chap. Part C: Specific Experimental Environments and Techniques, Springer, Berlin Heidelberg, 2007.

[13] Drela, M. and Giles, M. B., "Viscous-Inviscid Analysis of Transonic and Low Reynolds Number Airfoils," *AIAA*, Vol. 25, 1987, pp. 1347–1355.

[14] Brooks, T. F., Pope, D. S., and Marcolini, M. A., "Airfoil Self-Noise and Prediction," Tech. Rep. 1218, NASA Reference Publication, 1989.

[15] Herrig, A., "Trailing Edge Noise Measurements of a NACA 0012 Airfoil," Tech. rep., University of Stuttgart, Institute of Aerodynamics and Gas Dynamics, April 2007, Part III b.

[16] Corcos, G. M., "Resolution of Pressure in Turbulence," *Journal of the Acoustical Society of America*, Vol. 35, No. 2, 1963, pp. 192–199.

[17] Corcos, G. M., "The Resolution of Turbulent Pressures at the Wall of a Boundary Layer," *Journal of Sound and Vibration*, Vol. 6, No. 1, 1967, pp. 59–70.

[18] Lueptow, R. M., "Transducer Resolution and the Turbulent Wall Pressure Spectrum," *Journal of the Acoustical Society of America*, Vol. 97, No. 1, 1995, pp. 370–378.

[19] Löfdahl, L., Kälvesten, E., and Stemme, G., "Small Silicon Pressure Transducers for Space-Time Correlation Measurements in a Flat Plate Boundary Layer," *Journal of Fluids Engineering*, Vol. 118, 1996, pp. 457–463.

[20] Schewe, G., "On the structure and resolution of wall-pressure fluctuations associated with turbulent boundary-layer flow," *Journal of Fluid Mechanics*, Vol. 134, 1983, pp. 311–328.

[21] Bull, M. and Thomas, A., "High-Frequency Wall-Pressure Fluctuations in Turbulent Boundary Layers," *Physics of Fluids*, Vol. 19, No. 4, April 1976, pp. 597–599.

[22] Kamruzzaman, M., Herrig, A., Lutz, T., Würz, W., Krämer, E., and Wagner, S., "Comprehensive Evaluation and Assessment of Trailing Edge Noise Prediction Based on Dedicated Measurements," Third International Conference on Wind Turbine Noise, Aalborg, Denmark, 17.–19.06. 2009.

[23] Wilcox, D. C., *Turbulence Modeling for CFD*, DCW Industries, 2nd ed., 1998.

[24] Kamruzzaman, M., Lutz, T., Herrig, A., and Krämer, E., "RANS Based Prediction of Airfoil Trailing Edge Far-Field Noise: Impact of

Isotropic & Anisotropic Turbulence," 14th AIAA/CEAS Aeroacoustics Conference (29th AIAA Aeroacoustics Conference), Vancouver, Canada, 5–7 May 2008, AIAA-2008–2867.

[25] Kamruzzaman, M., Lutz, T., Ivanov, A., Herrig, A., and Krämer, E., "Evaluation of Measured Anisotropic Turbulent Two-Point Correlation Data for the Accurate Prediction of the Turbulence Noise Sources," 15th AIAA/CEAS Aeroacoustics Conference (30th AIAA Aeroacoustics Conference), Miami, Florida, 11–13 May 2009, AIAA 2009–3313.

[26] Parchen, R., "Progress Report DRAW, A Prediction Scheme for Trailing Edge Noise Based on Detailed Boundary-Layer Characteristics," Tech. Rep. HAG-RPT-980023, TNO Institute of Applied Physics, 1998.

[27] Hinze, J. O., *Turbulence*, McGraw-Hill, New York, 1975.

[28] Howe, M., "A Review of the Theory of Trailing Edge Noise," *Journal of Sound and Vibration*, Vol. 61, No. 3, 1978, pp. 437–465.

[29] Goody, M. C., *An Experimental Investigation of Pressure Fluctuations in Three-Dimensional Turbulent Boundary Layers*, Ph.D. thesis, Virginia Polytechnic Institute and State University, Sep. 17 1999.

[30] Herr, M., "Design Criteria for Low-Noise Trailing-Edges," 13th AIAA/CEAS Aeroacoustics Conference, Rome, Italy, May 21–23 2007, AIAA 2007–3470.

[31] Lee, Y.-T., Blake, W. K., and Farabee, T. M., "Modeling of Wall Pressure Fluctuations Based on Time Mean Flow Field," *Journal of Fluids Engineering*, Vol. 127, March 2005, pp. 233–240.

[32] Kamruzzaman, M., Lutz, T., and Krämer, E., "An Approach to RANS Based Prediction of Airfoil Trailing Edge Far-Field Noise," Second International Meeting on Wind Turbine Noise, Lyon, France, September 20–21 2007.

[33] Herrig, A., Würz, W., Krämer, E., and Wagner, S., "New CPV-Results of NACA 0012 Trailing-Edge Noise," Int. Conference on Methods of Aerophysical Research ICMAR, Novosibirsk, 30.06.–06.07. 2008.

[34] Howe, M. S., *Acoustics of Fluid-Structure Interactions*, Cambridge University Press, 2008.

[35] Howe, M. S., "Edge-Source Acoustic Green's Function for an Airfoil of Arbitrary Chord, with Application to Trailing-Edge Noise," *Quarterly Journal of Mechanics and Applied Mathematics*, Vol. 54, No. 1, Feb. 2001, pp. 139–155.

[36] Amiet, R., "Noise Due to Turbulent Flow Past a Trailing Edge," *Journal of Sound and Vibration*, Vol. 47, No. 3, 1976, pp. 387–393.

[37] Amiet, R. K., "Effect of the Incident Surface Pressure Field on Noise Due to Turbulent Flow Past a Trailing Edge," *Journal of Sound and Vibration*, Vol. 57, No. 2, 1978, pp. 305–306, Letters to the editor.

FANS SINGING NOT BEING HEARD

Manchester United have appointed an acoustic engineer to try and find out why singing at Old Trafford does not carry to all areas of the ground. The sound specialist has attended one game this season and will gather information at others in an attempt to pinpoint the problem. Noise levels at the stadium have been derided by opposition supporters and United fan groups.